Available online at www.sciencedirect.com
SCIENCE DIRECT®
Environmental Pollution 135 (2005) 65–72
ENVIRONMENTAL POLLUTION
www.elsevier.com/locate/envpol

Interaction of limestone grains and acidic solutions from the oxidation of pyrite tailings

M. Simón[a,*], F. Martín[b], I. García[a], P. Bouza[c], C. Dorronsoro[b], J. Aguilar[b]

[a]Departamento de Edafología, EPS-CITE IIB, Cañada San Urbano, Universidad de Almería, 04120 Almería, Spain
[b]Departamento de Edafología, Facultad de Ciencias, Universidad de Granada, 18002 Granada, Spain
[c]Centro Nacional Patagónico, CONICEF, Boulevard Brown s/n, 9120 Puerto Madryn, Chubut, Argentina

Received 9 April 2004; accepted 15 October 2004

Basaluminite, schwertmannite and jarosite armored the limestone grains, and almost all trace elements co-precipitated, but the precipitation of As and Pb tended to decrease as the pH rose.

Abstract

To characterise the coatings formed and to analyse element partitioning between the aqueous and solid phase, suspensions were prepared with four grain sizes of limestone and three different amounts of acidic solution from oxidized pyrite tailings. In all cases, red coatings with three different layers covered the grain surface, sealing off the acidic solution. The inner layer was composed mainly of basaluminite, the middle layer of schwertmannite, and the outer layer of gypsum and jarosite. Zn, Cd and Tl were co-precipitated by Fe and Al; As and Pb were co-precipitated almost completely by Fe; and Cu formed mainly Cu sulphates. All trace elements reached almost total precipitation at pH 6.3, but the precipitation of As and Pb tended to decrease as the pH rose. Consequently, liming should be calculated so that the soil pH does not exceed 6.3. This calculation should take into account that the armouring of the limestone grains can cause underestimations in the amount of liming material needed.

Keywords: Tailings oxidation; Pollutants; Limestone; Coatings; Element precipitation

1. Introduction

Soil pollution caused by tailings or acidic water from sulphide-rich mines is a growing worldwide problem of biogeochemical complexity involving hydration, hydrolysis and oxidation. When the tailings from a pyrite mine are exposed to oxygen and water, sulphides oxidize to sulphates, the pH falls markedly as a result of the formation of sulphuric acid, and the pollutants solubilize (Förstner and Wittmann, 1983). In the case of pyrite, the most abundant sulphide in these tailings, the oxidation can be represented by the following reactions:

$$2FeS_{2(s)} + 7O_{2(g)} + 2H_2O \rightarrow 2Fe^{2+}_{(aq)} + 4SO^{2-}_{4(aq)} + 4H^{+}_{(aq)} \quad (1)$$

$$4Fe^{2+}_{(aq)} + O_{2(g)} + 4H^{+}_{(aq)} \rightarrow 4Fe^{3+}_{(aq)} + 2H_2O \quad (2)$$

The Fe^{3+} released in reaction (2) may hydrolyse to form ferric hydroxide:

$$Fe^{3+}_{(aq)} + 3H_2O \rightarrow Fe(OH)_{3(s)} + 3H^{+}_{(aq)} \quad (3)$$

or it may oxidize additional pyrite by the reaction:

$$FeS_{2(s)} + 14Fe^{3+}_{(aq)} + 8H_2O \rightarrow 15Fe^{3+}_{(aq)} + 2SO^{2-}_{4(aq)} + 16H^{+}_{(aq)} \quad (4)$$

Reaction (2) is very slow at pH < 4.0 and has been described as the rate-determining step in pyrite oxidation (Singer and Stumm, 1970).

* Corresponding author. Tel.: +34 950 015923; fax: +34 950 015319.
E-mail address: msimon@ual.es (M. Simón).

0269-7491/$ - see front matter © 2004 Elsevier Ltd. All rights reserved.
doi:10.1016/j.envpol.2004.10.013

When this acidic solution from pyrite-tailings oxidation infiltrates the soil, the H^+ are partially neutralized either by exchangeable bases, by weathering of silicate mineral or, more intensely, by carbonates (Cravotta and Trahan, 1999). Neutralization decreases the concentration of dissolved elements due to precipitation, co-precipitation and adsorption processes (Xu et al., 1997). For this reason, one of the most widespread remedial actions is liming. In general, the potential acidity of 1 g of pyritic sulphur is neutralized by approximately 3 g of $CaCO_3$ (Williams et al., 1982). Nevertheless, when these acidic solutions, highly concentrated in Fe and S interact with the carbonate-mineral surface, the carbonate particle becomes coated with gypsum and amorphous ferric oxyhydroxides formed from the reaction (Ritsema and Groenenberg, 1993; Al et al., 2000):

$$Fe^{3+}_{(aq)} + 2SO^{2-}_{4(aq)} + H^{+}_{(aq)} + 2CaCO_{3(s)} + 5H_2O \rightarrow Fe(OH)_{3(s)} + 2CaSO_4{\cdot}2H_2O_{(s)} + 2CO_{2(g)} \quad (5)$$

This diminishes the rate of carbonate dissolution and reduces the neutralizing power of the calcite (Ziemkiewicz et al., 1997), causing inaccuracy in the quantification of the liming material required (Barnhisel et al., 1982).

Evangelou (1995) reported that $Fe(OH)_3$ precipitates are formed on the surface of limestone through adsorption of Fe(II), followed by oxidation. However, under anoxic conditions, where iron oxidation is negligible, the coatings are formed fundamentally by Al-hydroxysulfates (Robbins et al., 1999). In addition to gypsum, the main minerals that form part of the coating are ferrihydrite, jarosite-group minerals, lepidocrocite, schwertmannite, goethite and aluminite (Loeppert and Hossner, 1984; Robbins et al., 1999; Al et al. (2000).

In natural streams, because of the gradient in pH, the Al- and Fe-precipitates are found spatially separated (Bigham and Nordstrom, 2000). A similar spatial separation of the precipitates in the coatings formed on limestone surface has been found by Hammarstrom et al. (2003), distinguishing a series of more or less continuous layers: inner gypsum rind, thin Al-rich layer, and outermost Fe hydroxysulfate. The sequence of deposition of these layers appears to be related to the pH, increasing the molar Al:Fe ratio with increasing pH (Cravotta and Trahan, 1999).

Many researchers have described the reactions of some metals with iron-coated. Thus, Cravotta and Trahan (1999) revealed that Fe- and Al-coated limestone promotes sorption and co-precipitation of Cu, Co, Ni and Zn. Al et al. (2000) studied the chemical composition and mineralogy of coatings on carbonate minerals from mine tailings, and the results suggest that the Pb and Zn were adsorbed, Cu and Cd co-precipitated, and As was adsorbed and/or co-precipitated by these coatings formed principally by jarosite-group minerals, goethite, akaganéite and amorphous Fe oxyhydroxides.

Nevertheless, the interactions of the carbonate-mineral surface with the elements released by oxidation of the pyrite tailings are likely to be very complex, and the details are partly unknown. In the present work, limestone of different grain sizes were placed in contact with an acidic solution from the oxidation of pyrite tailings. The aim is to contribute to the knowledge of the morphology and composition of the coatings formed, as well as to analyse element partitioning between the aqueous and solid phase. The results could be used to maximize efficiency in liming practices for the remediation of soils affected by this type of pollution.

2. Methods

2.1. Preparation of suspensions

Four different grain sizes of limestone were placed in contact with three different amounts of an acidic solution from oxidized pyrite tailings. The most abundant elements present in the pyrite tailings were: S (30.0–40.0%), Fe (30.0–37.0%), Al (0.60–2.95%), Pb (0.60–1.00%), Zn (0.60–0.85%), As (0.15–0.45%), and Cu (0.10–0.25%). Other mineralogical and chemical characteristics of the pyrite tailings can be found in Simón et al. (1998) and López–Pamo et al. (1999). Limestone containing 96.8% $CaCO_3$ equivalent was ground and sieved at the following grain sizes: coarse (2–0.5 mm), medium (0.5–0.1 mm), fine (0.1–0.05 mm), and very fine (<0.05 mm). The specific surface area (SA) of each fraction, determined by weighting the water adsorbed by the samples from a solution saturated with $CaCl_2$ (Keeling, 1961), was 0.733, 1.031, 2.024, and 2.534 m^2/g, respectively. Next, a pollutant solution was prepared by adding 1000 cm^3 of H_2O_2 (15%) to 10 g of pyrite tailings from the Aznalcóllar mine (SE Spain) and after three days the solution was removed, the pH measured (1.8) and the sediment discarded. The element concentration in the solution (mg/L) was: SO_4 12 335, Fe 3700, Al 510, Zn 245, Cu 51.9, As 48.5, Pb 5.74, Cd 1.22, and Tl 0.09. Afterwards, 60, 100 and 200 cm^3 of the acidic solution were added, respectively, to 10 g of each grain-size fraction. After three days, each suspension was measured for pH and then centrifuged at 3000 rpm for 10 min to separate the solid from the liquid phase. The suspensions (S) were labelled by a letter representing the grain size of the limestone and by a number representing the cm^3 of acidic solution/g dry limestone (e.g., the suspension SM10 was prepared with 100 cm^3 of acidic solution and 10 g of medium-size limestone).

2.2. Liquid-phase analysis

In the liquid phase of the suspensions and in the acidic solution, the sulphate was determined by ion

chromatography in a Dionex model DX-120 instrument, Fe and Al were measured by atomic absorption spectroscopy in a PERKIN-ELMER 305B spectrophotometer, and the trace elements by inductively coupled plasma mass spectrometry (ICP-MS) with a PE SCIEX-ELAN 5000 spectrometer. The amount of each element precipitated was calculated by the difference between the concentration in the acidic solution and in the liquid phases of the suspensions.

2.3. Solid-phase analysis

The $CaCO_3$-equivalent content of the limestone and the different particle sizes in suspensions were estimated from the pressure of CO_2 formed after the samples reacted with HCl:H_2O (1:1) (Williams, 1948). The gypsum content of the solid phases was determined by dissolution in water of total sulphates followed by precipitation with acetone (Bower and Huss, 1948). The limestone grains after reaction with the acidic solution, as isolated grains and polished samples, were studied by Scanning Electron Microscopy (SEM) in a CARL ZEISS DSM 950 instrument with a back-scattered electron (BSE) detector and a Tracor Northern 523 X-ray energy dispersive spectrometry (EDS) with an Oxford Link ISIS microanalysis system. For X-ray diffraction, a Philips PW-1700 instrument with CuKα radiation was used.

3. Results

3.1. Weathering of the $CaCO_3$ and coating formed

The interaction of the acidic solution with the limestone grains partially weathered the $CaCO_3$ (between 0.15 g in suspension SC6 and 0.83 g in suspension SVF20), and formed continuous red coatings on the surface of all the grains (Fig. 1). The quantity of $CaCO_3$ weathered (W_{CaCO_3}) was correlated significantly ($p < 0.001$) with the cm^3 of acid solution/g dry limestone of each suspension (S) and with the Fe precipitated mg/g dry limestone (P_{Fe}) by the multiple regression:

$$W_{CaCO_3}\,(g) = 0.008S\,(cm^3/g) + 0.018P_{Fe}\,(mg/g) - 0.020$$
$$r^2 = 0.999 \qquad (6)$$

By SEM-EDS analysis, the coatings (Fig. 2a) showed tabular crystals composed of S and Ca (gypsum), aggregated microcrystals of Fe with S, and globules composed of Fe, Al and S embedded in a cracked amorphous mass (Fig. 2b). A backscattered electron scanning (BES) micrograph of a polished section of the coatings (Fig. 2c) revealed that these coatings were composed of three different layers: an irregular inner layer (I), closer to the limestone–grain surface; a middle layer (M) containing the globules, which appeared to be hollow; and an outer layer with the much larger gypsum crystals (Og) together with the microcrystal aggregates (Om). The distribution map of Al, Fe and S in the polished section of the micrograph 2c (Fig. 2d, e and f, respectively) reveals that Al was concentrated in the inner layer as well as in the fractures of the limestone, Fe accumulated in the middle layer as well as in the microcrystals of the outer layer, while S was present in all layers, especially in the gypsum crystals.

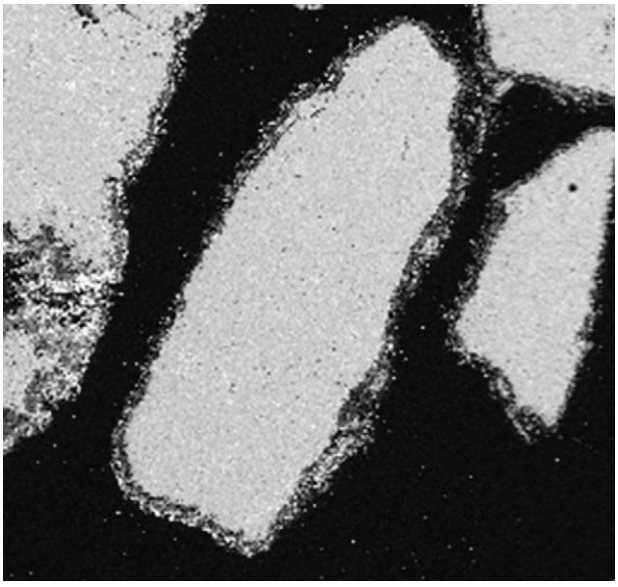

Fig. 1. Polished section of medium-sized limestone grains in suspension SM20 showing continuous coatings on the surface. Frame length 500 μm.

The quantitative analysis of these layers (3 replicates) by EDS (Table 1) confirmed that the inner layer was composed fundamentally of Al, and had the highest Zn concentration, whereas the middle layer and the microcrystals of the outer layer were composed mainly of Fe. Meanwhile, As was concentrated in the layers where Fe was the majority component.

3.2. Suspension pH and precipitation of the elements

The pH values of the suspensions (Table 2) were significantly ($p < 0.01$) and directly correlated to the specific surface area of the particles (SA) but inversely to the cm^3 of the acidic solution/g dry limestone (S) by the multiple regression:

$$pH = 0.826SA\,(m^2/g) - 0.036S\,(cm^3/g) + 4.36$$
$$r^2 = 0.793 \qquad (7)$$

The amounts of SO_4 and Fe precipitated mg/g dry limestone (P_{SO_4} and P_{Fe}) were relatively high, the P_{SO_4}

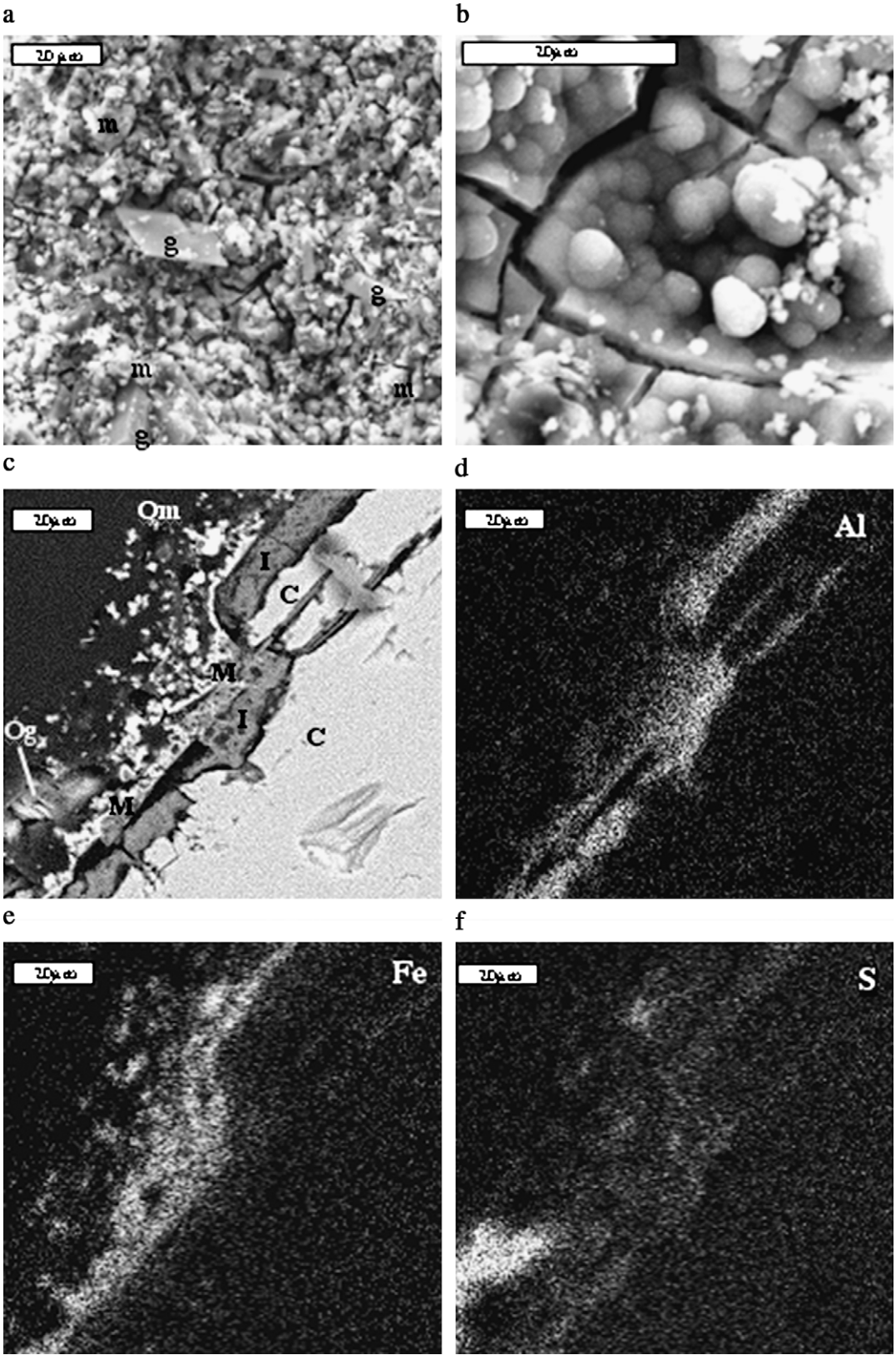

Fig. 2. (a) SEM-EDS analysis of the coatings on the medium-sized grain in suspension SM20, showing tabular crystals (g) composed of S and Ca and aggregated microcrystals (m) of Fe with S; both deposited on a cracked amorphous mass. (b) Detail of the cracked amorphous mass with embedded globules composed of Fe, Al and S. (c) Backscattered electron scanning (BES) micrograph of a polished section of the coatings around the limestone grains (C) showing three different layers: an irregular inner layer (I); a middle layer (M) containing the globules; and an outer layer with gypsum crystals (Og) and microcrystal aggregates (Om). The micrographs d, e and f represent the distribution of Al, Fe and S by EDS, respectively, in the polished section of the micrograph c.

Table 1
Mean content and standard deviation (SD) of some elements in the different layers of the coatings by EDS

Layers	Al (%)		Fe (%)		Zn (%)		As (%)		S (%)	
	Mean	SD	Mean	SD	Mean	SD	Mean	SD	Mean	SD
Inner (I)	31.4	3.1	3.20	0.09	0.87	0.14	0.03	0.02	8.51	0.99
Middle (M)	6.89	0.24	26.7	1.8	0.34	0.06	2.25	0.11	2.88	0.21
Outer (Om)	0.88	0.13	32.5	2.6	0.11	0.02	3.02	0.18	11.3	0.6
Outer (Og)	0.16	0.05	1.53	0.14	nd	–	nd	–	47.0	2.2

nd = not detected.

values ranging from 25 mg/g to 127 mg/g, and the P_{Fe} from 7 to 38 mg/g. Far lower amounts of Al, Cu, Zn and As precipitated mg/g dry limestone (P_{Al}, P_{Cu}, P_{Zn}, and P_{As}), values ranging between 0.03 and 2.4 mg/g; meanwhile, the quantities of Cd, Tl and Pb precipitated mg/g dry limestone (P_{Cd}, P_{Tl}, P_{Al}) were lowest, ranging between 10^{-4} and 0.11 mg/g (Table 2).

The P_{SO_4}, P_{Fe} and P_{Al} values correlated significantly ($p < 0.001$) with the pH and the total SO_4, Fe and Al mg/g dry limestone (T_{SO_4}, T_{Fe} and T_{Al}, respectively); in addition, P_{Al}, also correlated with the SA (m^2/g) of the grains of limestone. The multiple regressions were:

$$P_{SO_4}\,(\mathrm{mg/g}) = 0.43 T_{SO_4}\,(\mathrm{mg/g}) + 25.38\mathrm{pH} - 134.5 \quad r^2 = 0.984 \tag{8}$$

$$P_{Fe}\,(\mathrm{mg/g}) = 0.43 T_{Fe}\,(\mathrm{mg/g}) + 8.10\mathrm{pH} - 42.73 \quad r^2 = 0.991 \tag{9}$$

$$P_{Al}\,(\mathrm{mg/g}) = 0.05 T_{Al}\,(\mathrm{mg/g}) + 0.29\mathrm{pH} + 0.21\mathrm{SA}\,(\mathrm{m^2/g}) - 1.67 \quad r^2 = 0.972 \tag{10}$$

The SO_4 precipitated as gypsum mg/g dry limestone (PG_{SO_4}) was significantly related ($p < 0.001$) to P_{SO_4} by the linear regression:

$$PG_{SO_4}\,(\mathrm{mg/g}) = 0.63 P_{SO_4}\,(\mathrm{mg/g}) - 0.12 \quad r^2 = 0.997 \tag{11}$$

Meanwhile, the SO_4 that precipitated in a different form of gypsum, presumably as hydroxysulphates (PHS_{SO_4}), was significantly related ($p < 0.001$) to P_{Fe} by the linear regression:

$$PHS_{SO_4}\,(\mathrm{mg/g}) = 1.24 P_{Fe}\,(\mathrm{mg/g}) - 1.55 \quad r^2 = 0.980 \tag{12}$$

The trace elements Zn, Cd and Tl precipitated mg/g dry limestone (P_{Zn}, P_{Cd} and P_{Tl}) were significantly related ($p < 0.001$) to P_{Fe} and P_{Al} by the multiple regressions:

$$P_{Zn}\,(\mathrm{mg/g}) = 0.02 P_{Fe}\,(\mathrm{mg/g}) + 1.61 P_{Al}\,(\mathrm{mg/g}) - 0.17 \quad r^2 = 0.995 \tag{13}$$

$$P_{Cd}\,(\mathrm{mg/g}) = 0.26\times10^{-3} P_{Fe}\,(\mathrm{mg/g}) + 9.61\times10^{-3} P_{Al}\,(\mathrm{mg/g}) - 2.53\times10^{-3} \quad r^2 = 0.967 \tag{14}$$

$$P_{Tl}\,(\mathrm{mg/g}) = 0.02\times10^{-3} P_{Fe}\,(\mathrm{mg/g}) + 0.15\times10^{-3} P_{Al}\,(\mathrm{mg/g}) - 0.06\times10^{-3} \quad r^2 = 0.995 \tag{15}$$

In addition, the As and Pb precipitated mg/g dry limestone (P_{As} and P_{Pb}) were significantly ($p < 0.001$)

Table 2
The pH of the suspensions and elements precipitated in mg/g dry limestone

Sample	pH	SO_4^{2-}	Fe	Al	Cu	Zn	As	Cd	Tl	Pb
SC6	4.9	25.7	7.1	0.08	0.26	0.08	0.29	0.002	0.0001	0.034
SM6	5.9	45.1	14.0	0.49	0.31	0.95	0.29	0.006	0.0003	0.034
SF6	6.1	47.8	16.7	0.57	0.31	1.12	0.29	0.007	0.0003	0.034
SVF6	6.2	51.9	17.5	0.69	0.31	1.27	0.29	0.007	0.0003	0.034
SC10	4.6	40.3	11.4	0.07	0.35	0.03	0.48	0.001	0.0001	0.056
SM10	5.9	64.2	19.0	0.55	0.52	1.17	0.48	0.008	0.0004	0.057
SF10	6.0	70.6	20.0	0.77	0.52	1.43	0.48	0.010	0.0004	0.057
SVF10	6.1	75.6	23.2	0.95	0.52	1.72	0.48	0.012	0.0004	0.057
SC20	3.8	61.7	19.2	0.07	0.31	0.28	0.96	0.003	0.0002	0.106
SM20	5.6	111.0	33.6	0.66	1.03	1.52	0.97	0.011	0.0006	0.113
SF20	5.8	120.5	36.8	0.94	1.04	2.14	0.97	0.016	0.0007	0.113
SVF20	5.9	127.1	38.0	1.14	1.04	2.38	0.97	0.020	0.0007	0.113

and directly related to P_{Fe} but inversely to pH by the multiple regressions:

$$P_{As}\,(mg/g) = 0.03P_{Fe}\,(mg/g) - 0.25pH + 1.30 \quad r^2 = 0.991 \tag{16}$$

$$P_{Pb}\,(mg/g) = 0.004P_{Fe}\,(mg/g) - 0.028pH + 0.15 \quad r^2 = 0.991 \tag{17}$$

Finally, the Cu precipitated mg/g dry limestone (P_{Cu}) was significantly ($p < 0.001$) and directly related to PHS_{SO_4} and pH but inversely to P_{Al} by the multiple regression:

$$P_{Cu}\,(mg/g) = 0.03PHS_{SO_4}\,(mg/g) + 0.18pH - 0.55P_{Al}\,(mg/g) - 0.97 \quad r^2 = 0.960 \tag{18}$$

4. Discussion

The H^+ present in the suspensions constituted the primary agent that caused the weathering of $CaCO_3$ by the reaction:

$$CaCO_{3(s)} + 2H^+_{(aq)} \rightarrow Ca^{2+}_{(aq)} + CO_{2(g)} + H_2O$$

Thus, Eq. (6) reveals that the $CaCO_3$ was weathered not only by the H^+ present in the acidic solution (S) but also by that formed during the oxidation and precipitation of iron (P_{Fe}, reactions (2) and (3)).

Because the H^+ interacted with the limestone grain surface, the weathering increased as the specific surface area enlarged, consequently raising the pH of the suspension (Eq. (7)). Nevertheless, most of the limestone in all the suspensions resisted weathering (between 99% of the SG6 suspension and 91% of the SVF20 suspension) despite the acidic pH (between 3.8 of the SG6 suspension and 6.2 of the SVF20 suspension). This together with the fact that the pH of the water (with pressure of CO_2 similar to that of the atmosphere ≈ 0.0003 atm) in equilibrium with $CaCO_3$ reaches 8.3 (Lindsay, 1979), seem to confirm that coatings sealed off the limestone grains from interacting with the solution.

The high concentration of Al in the inner layer is consistent with the lower pK_1 of Al^{3+} in relation to Fe^{2+} formed in the oxidation of pyrite (Reaction (1)), resulting in more extensive hydrolysis and rapid precipitation onto the limestone surface; later, the oxidation of Fe^{2+} to Fe^{3+} (Reaction (2)) would trigger the hydrolysis of Fe^{3+} (pK_1 lower than that of Al^{3+}) and precipitation onto the existing Al layer.

The mean molar ratio Al:S of the inner layer of the coatings was 4.4, implying that the mineral formed was probably basaluminite (Nordstrom and Ball, 1986). The molar ratio Fe:S of the middle was greater than 5, indicating the formation of schwertmannite (Bigham et al., 1996); meanwhile, the molar ratio Fe:S of the microcrystals of the outer layer was only 1.6, reflecting that the mineral formed was jarosite (Filipeck et al., 1987). The above results were supported by an X-ray diffractogram of a sample from the outer layer of coated particles (suspension SM20) gently brushed and screened (0.05 mm mesh size), indicating the presence of gypsum and jarosite.

Roughly 43% of T_{SO_4} and T_{Fe}, and only 5% of T_{Al} in the acidic solution was precipitated on limestone grains (Eqs. (8)–(10)), this quantity increasing with the pH and, in the case of Al, also with the specific surface area (SA). Because pH and SA were directly correlated (Eq. (7)), the increase in pH tended to raise P_{Al} values more than P_{Fe}, and the P_{Fe}:P_{Al} ratio decreased (Fig. 3). Consequently, the ratio between the basaluminite formed in the inner layer, on the one hand, and the schwertmannite and jarosites formed in the middle and outer layers, on the other hand, proved to be pH-dependent.

Approximately 63% of the P_{SO_4} formed gypsum (Eq. (11)). The remaining 37% must have precipitated as hydroxysulphates (PHS_{SO_4})—fundamentally as Fe hydroxysulphates, as reflected by the higher P_{Fe} than P_{Al} values (Table 2) and by the significant linear relationship between PHS_{SO_4} and P_{Fe} (Eq. (12)).

Zn, Cd and Tl were co-precipitated with Fe and Al (Eqs. (13)–(15)), although in all cases the regression coefficient of the P_{Al} was higher than that of the P_{Fe}, indicating that per unit of weight the P_{Al} co-precipitated more Tl (10-fold), and far more Cd (40-fold) and Zn (80-fold), than did the P_{Fe}. However, the higher P_{Fe} values (mean 21.4 mg/g) with respect to those of P_{Al} (mean 0.58 mg/g), together with the increase in the P_{Fe}:P_{Al} ratio as the pH decreased (Fig. 3), could mask this fact. Thus, although the ratio between the total amount of each metal (m) adsorbed by P_{Al} (Al_m) and P_{Fe} (Fe_m) in each suspension (estimated from the Eqs. (13)–(15)) increased as the pH rose (Fig. 4), the P_{Fe} co-precipitated more Tl than did the P_{Al} in all suspensions (Al_m:Fe_m ratio < 1) and more Zn in the suspensions with pH < 5.0.

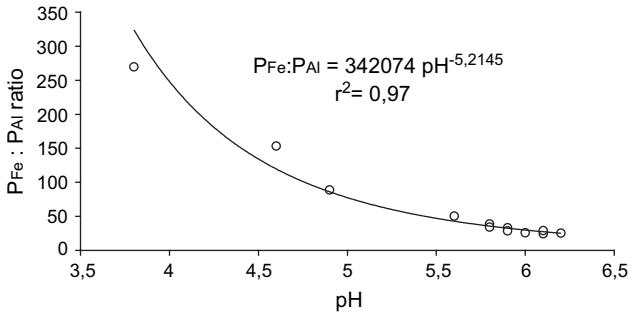

Fig. 3. Ratio between precipitated Fe and Al (P_{Fe}:P_{Al}) versus pH.

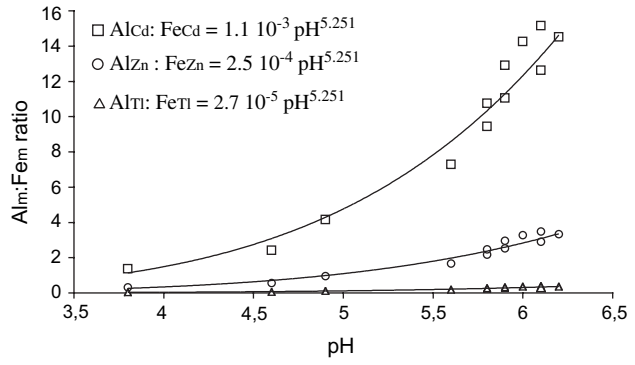

Fig. 4. Ratio between the total mg of Cd, Zn and Tl co-precipitated with Al (Al_m) and with Fe (Fe_m) versus pH.

In any case, the percentage of Zn, Cd and Tl precipitated with respect to the total dissolved in the acidic solution increased as the pH rose, although each element behaved differently (Fig. 5). Thus, the percentage of Zn precipitated was very low up to pH 5.4 (≈5%), afterwards increasing by approximately 9% per 0.1 unit of rise in pH until almost total precipitation at pH 6.4. The percentage of Cd precipitated was also very low at pH 4.6 (≈10%), while between pH 4.6 and 5.6 the values increased roughly 3.5% per 0.1 unit pH, and at pH > 5.6 the increase was 9% per 0.1 unit pH, approaching total precipitation at pH 6.3. The percentage of Tl resembled that of Cd at pH 4.6 but then increased by only 2.5% per 0.1 unit pH, implying almost total precipitation at pH > 8.0.

Pb and As were co-precipitated with Fe but the quantity precipitated decreased as pH increased (Eqs. (16) and (17)), results similar to those reported by Jones et al. (1997) and Tyler and Olsson (2001). Raven et al. (1998) indicated that the lower adsorption of As at high pH was attributable to the more negatively charged arsenate species repulsing the negatively charged surface sites. Consequently, although within the pH range of the suspensions (3.8–6.2) the percentages of As and Pb adsorbed were very high (>99.9% As and >98.0% Pb), according to the above, precipitation could decrease at pH > 6.5, increasing bioaccessibility (Yang et al., 2002).

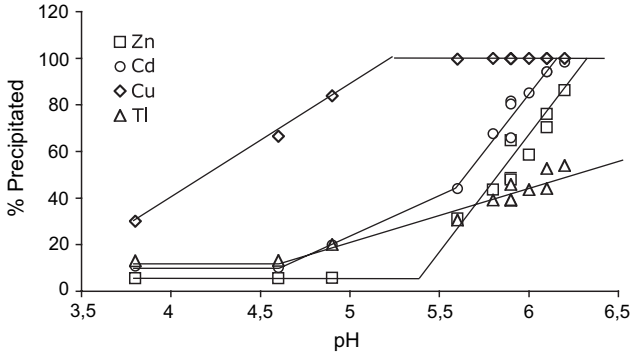

Fig. 5. Percentage precipitated of Zn, Cd, Tl and Cu versus pH.

The Cu enabled the formation of more or less complex Cu sulphates that increased as the pH rose, although Al appeared to compete with Cu in the metal-sulphate formation given that the P_{Cu} decreased as the basaluminite increased (Eq. (18)). In any case, the percentage of Cu that precipitated, 30% at pH 3.8, increased by approximately 5% per 0.1 unit pH to 5.3, whereupon adsorption stabilized at 99.5% (Fig. 5).

5. Conclusions

The interaction between limestone and the acidic solution from the oxidation of pyrite tailings raised the pH of the solution, inducing the precipitation of more or less complex sulphates which co-precipitated with almost all of the dissolved elements when the pH of the solution was around 6.3. However, the sulphates formed a grain coating that sealed off the limestone grains; therefore, fresh $CaCO_3$ is required to raise the pH of the solution. Consequently, in the remediation of soils contaminated by pyrite tailings, it should be taken into account that it is easy to underestimate the amount of liming material required. Armouring of the limestone grains could be counteracted by periodic tilling to break up the grain coatings.

Acknowledgments

We express our gratitude to the Science and Technology Ministry of Spain for supporting this study (Project REN2003-03268). Furthermore, we thank David Nesbitt for correcting the English version of the manuscript.

References

Al, T.A., Martin, C.J., Blowes, D.W., 2000. Carbonate–mineral/water interaction in sulfide-rich mine tailings. Geochimica et Cosmochimica Acta 64 (23), 3933–3948.

Barnhisel, R.I., Powell, J.L., Akin, G.W., Ebelhar, M.W., 1982. Characteristics and reclamation of acid sulfate mine spoils. In: Kral, D.M., Hawkins, S. (Eds.), Acid Sulfate Weathering. Soil Science Society of America, Madison, pp. 225–234.

Bigham, J.M., Nordstrom, D.K., 2000. Iron and aluminium hydroxysulphates from acid sulfate waters. In: Alpers, C.N., Jambor, J.L., Nordstrom, D.K. (Eds.), Sulfate Minerals, Reviews in Mineralogy and Geochemistry, vol. 40. Mineralogical Society of America, Washington, DC, pp. 351–403.

Bigham, J.M., Schwertmann, U., Traina, S.J., Winland, R.L., Wolf, M., 1996. Schwertmannite and the chemical modelling of iron in acid sulfate waters. Geochimica et Cosmochimica Acta 60 (12), 2111–2121.

Bower, C.A., Huss, R.B., 1948. Rapid conductometric method for estimating gypsum in soils. Soil Science 141, 99–204.

Cravotta, C.A., Trahan, M.K., 1999. Limestone drains to increase pH and remove dissolved metals from acidic mine drainage. Applied Geochemistry 14, 581–606.

Evangelou, V.P., 1995. Pyrite Oxidation and Its Control. CRC Press, Boca Raton, FL.

Filipeck, L.H., Nordstrom, D.K., Flicklin, W.H., 1987. Interaction of acid mine drainage with waters and sediments of West Squaw Creek in the West Shasta mining district, California. Environmental Science and Technology 21, 388–396.

Förstner, U., Wittmann, G.T.W., 1983. Metal Pollution in the Aquatic Environment. Springer-Verlag, Berlin.

Hammarstrom, J.M., Sibrell, Ph.L., Belkin, H.E., 2003. Characterization of limestone reacted with acid-mine drainage in a pulsed limestone bed treatment system at the Friendship Hill National Historical Site, Pennsylvania, USA. Applied Geochemistry 18, 1705–1721.

Jones, C.A., Inskeep, W.P., Neuman, D.R., 1997. Arsenic transport in contaminated mine tailings following liming. Journal of Environmental Quality 26, 433–439.

Keeling, P., 1961. The examination of clays by IL/MA. Transaction of the British Ceramic Society 60, 217–244.

Lindsay, W.L., 1979. Chemical Equilibria in Soil. John Wiley and Sons, New York.

Loeppert, R.H., Hossner, L.R., 1984. Reaction of Fe^{2+} and Fe^{3+} with calcite. Clays and Clays Minerals 32 (3), 213–222.

López-Pamo, E., Barettino, D., Antón-Pacheco, C., Ortiz, G., Arránz, J.C., Gumiel, J.C., Martínez-Pledel, B., Aparicio, M., Montouto, O., 1999. The extent of the Aznalcóllar pyritic sludge spill and its effects on soils. The Science of the Total Environment 242, 57–88.

Nordstrom, D.K., Ball, J.W., 1986. The geochemical behavior of aluminum in acidified surface waters. Science 232, 54–56.

Raven, K.P., Jain, A., Loeppert, R.H., 1998. Arsenite and arsenate adsorption on ferrrihydrite: kinetics, equilibrium, and adsorption envelopes. Environmental Science and Technology 32 (3), 344–349.

Ritsema, C.J., Groenenberg, J.E., 1993. Pyrite oxidation, carbonate weathering, and gypsum formation in a drained potential acid sulfate soil. Soil Science Society of America Journal 57, 968–976.

Robbins, E.I., Cravotta III, C.A., Savela, C.E., Nord Jr., G.L., 1999. Hydrobiogeochemical interactions in 'anoxic' limestone drains for neutralization of acidic mine drainage. Fuel 78, 259–270.

Simón, M., Ortiz, I., García, I., Fernández, E., Fernández, J., Dorronsoro, C., Aguilar, J., 1998. El desastre Ecológico de Doñana. Edafología 5, 153–161.

Singer, P.C., Stumm, W., 1970. Acidic mine drainage: the rate-determining step. Science 167, 1121–1123.

Tyler, G., Olsson, T., 2001. Concentration of 60 elements in the soil solution as related to the soil acidity. European Journal of Soil Science 52, 151–165.

Williams, D.E., 1948. A rapid manometric method for determination of carbonate in soils. Soil Science Society American Proceeding 13, 127–129.

Williams, E.G., Rose, A.W., Parizek, R.R., Waters, S.A., 1982. Factors controlling the generation of acid mine drainage. Final Report on US Bureau of Mines Research Grant n° G51055086. Pennsylvania State University.

Xu, Y., Schwartz, F.W., Traina, S.J., 1997. Treatment of acidic-mine water with calcite and quartz. Environmental Engineering Science 14 (3), 141–152.

Yang, J., Barnett, M.O., Jardine, P.M., Basta, N.T., Casteel, S.W., 2002. Adsorption, sequestration and bioaccessibility of As(V) in soils. Environmental Science and Technology 36 (21), 4562–4569.

Ziemkiewicz, P.F., Skousen, J.G., Brant, D.L., Sterner, P.L., Lovett, R.J., 1997. Acid mine drainage with armored limestone in open limestone channels. Journal of Environmental Quality 26, 1017–1024.